CONTRIBUTIONS TO THE 17th INTERNATIONAL

CONFERENCE ON COSMIC RAYS

PARIS, FRANCE, JULY 1981

PP 81-205

UNIVERSITY OF MARYLAND
DEPARTMENT OF PHYSICS AND ASTRONOMY

COLLEGE PARK, MARYLAND

TABLE OF CONTENTS

OBSERVATIONS OF INTERPLANETARY ENERGETIC CHARGED PARTICLES FROM GAMMA-RAY LINE SOLAR FLARES

M.E. Pesses[1], B. Klecker[2], G. Gloeckler[1], and D. Hovestadt[2]

1. University of Maryland, College Park, Maryland 20742 USA
2. Max-Planck-Institut fur Extraterr. Physik, 8046 Garching, FRG

ABSTRACT

Observations of interplanetary energetic ions (H^+; $5 \leq E_H \leq 20$ MeV, He, C, O, Fe; $1 \lesssim E_i \lesssim 20$ MeV/nucleon) and electrons ($115 \leq E_e \leq 1300$ keV) from the 7 June, 21 June and 1 July 1980 γ-ray line solar flares are presented. The observations are from the Max-Planck-Institut/University of Maryland Ultra Low Energy Wide Angle Telescope aboard the ISEE-3 spacecraft. Both June flares produced relatively low intensity proton events at earth with peak intensities at 10-20 MeV $\sim 5 \times 10^{-2}$ protons $(cm^2 \text{ sec sr MeV})^{-1}$. Neither flare showed evidence of being enriched in either ^{3}He or Fe at $\sim$1 MeV/nucleon. The 1 July flare produced no observable ion or electron enhancements.

1. Introduction

Gamma-ray line emission from the sun was first observed in the great flares of 4 August and 7 August 1972 by Chupp et al.[1] Solar flares which produce γ-ray line emission provide a unique opportunity to study ion acceleration phenomena in flares. For only in such flares can information on the accelerated ion population within the solar atmosphere be obtained by direct observations.[2] This information combined with interplanetary energetic charged particle data can provide the most stringent constraints on ion acceleration phenomena.

The purpose of this brief paper is to present the initial results from the Max-Planck-Institut (MPI)/University of Maryland (UM) experiments on ISEE-3 on interplanetary energetic charged particles from the 7 June, 21 June and 1 July γ-ray line solar flares (GRLF).

2. Instrument Description

The energetic particle data discussed in this paper are from the MPI/UM Ultra Low Energy Wide Angle Telescope (ULEWAT), aboard the ISEE-3 spacecraft. The ULEWAT is a double dE/dx versus E, thin-window, flow-through proportional counter/solid state detector composition telescope. For a detailed description of ULEWAT see Hovestadt et al.[3]

3. Gamma-Ray Line Flare Identification

From the launch of the Solar Maximum Mission (SMM) spacecraft, 14 February 1980, through the period for which we have reduced our ULEWAT data, 20 July 1980, the SMM Gamma Ray Experiment (GRE) detected γ-ray

lines from three flares. The photon characteristics of these GRLF are summarized in Table 1.

Table 1. Gamma-Ray Line Flare Characteristics

Flare Date (1980)	H_α onset	X-ray Max	Location	Active Region	Classification H_α	Classification X-ray	Radio Bursts(1) II	Radio Bursts(1) III	Radio Bursts(1) IV	$^2H^* \rightarrow {}^2H + 2.2$ MeV Intensity(2)(3) Peak/Aug. 72	$^2H^* \rightarrow {}^2H + 2.2$ MeV Intensity(2)(3) Integral/Aug. 72
7 June	0309	0312	N14W70	2495	SB	M7	Y	Y	Y	~1	$\sim 10^{-1}$
21 June	0048	0119	N17W91	2502	1B	X2	Y	Y	Y	?(4)	
1 July(5)	1618	1626	S12W38	2544	1B	X2	Y	Y	N	~1/2	$\sim 5\times 10^{-2}$

(1) Y refers to observed, N not observed.
(2) Values given are for the ratio of peak [integral] intensity of the $^2H^* \rightarrow {}^2H + \gamma(2.2\ MeV)$ line to that observed in the 4 August 1972 GRLF.
(3) From Ryan et al.[4]
(4) The peak of the 2.2 MeV line was obscured by continuum γ-rays. When the line emerged from continuum the intensity was one 1 July 1980 GRLF.
(5) This GRLF was also a white light flare.[5]

We have identified the interplanetary energetic particle event depicted in Figure 1 as originating from the 7 June 1980 GRLF. This identification is based on: (1) a time delay of 21 ± 1 minutes between the hard x-ray maximum at the sun and the arrival time of 0.44-1.3 MeV electrons at ISEE-3, (2) the W70° heliographic longitude of the GRLF, and (3) the absence of any other large hard x-ray flares within two hours of the observed particle event. No solar wind data at earth are available for this period.

Figure 1 presents 3 hour averages of several ULEWAT counting rates. The solid circles represent $Z > 2$ ions with $12 \lesssim E_i \lesssim 40$ MeV/nuc. The triangle represents He with $5 \leq E_\alpha \leq 20$ MeV. The short horizontal line in the lower right hand corner gives the upper-limit for He 5-20 MeV/nuc and $Z > 2$ ~12-40 MeV/nuc particles.

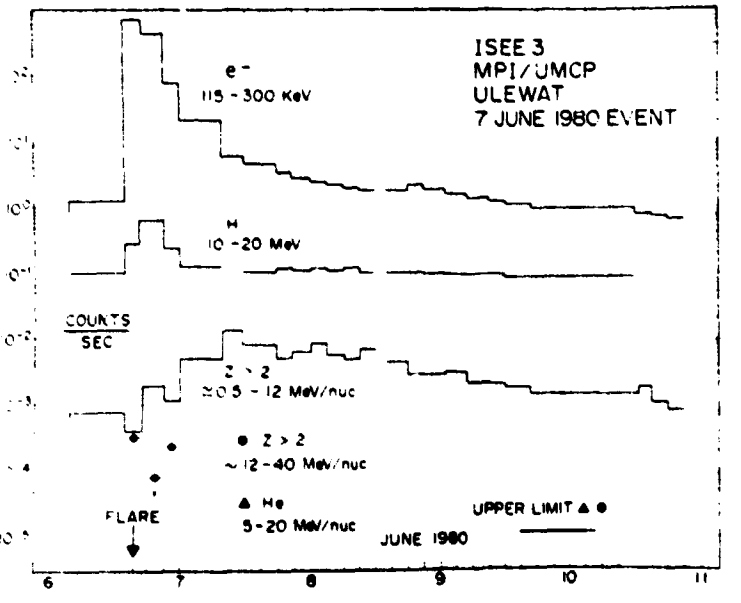

Figure 1

We have tentatively identified the first of two interplanetary energetic particle enhancements depicted in Figure 2 as originating from the 21 June 1980 GRLF. The onset of the second enhancement is indicated by the factor of two increase in 115-300 KeV electrons and 10-20 MeV protons intensity at ~0 UT on 23 June. The onset for the $Z > 2$ (≈0.5-12 MeV/nuc) ions in this enhancement is not as clear and probably occurs ~3-6 UT on 23 June. The identification of the first event in Figure 2 with the 21 June 1980 GRLF is based on: (1) a time delay of 34 ± 1 minutes between the hard x-ray minimum at the sun and the arrival of 0.44-1.3 MeV electrons at ISEE-3, and (2)

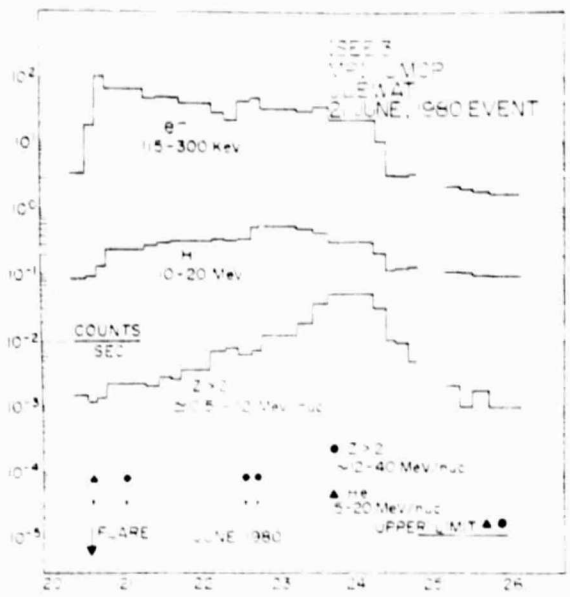

Figure 2

the W91° heliographic longitude of the GRLF. No solar wind data, at earth, are available for this period.

We are unable to find any interplanetary energetic particle event that is associated with the 1 July GRLF, in either the ULEWAT data or data from the UM/MPI instrustrument aboard the earth-orbiting IMP-8 spacecraft. No solar wind data, at earth, is available for 1 July 1980. However, there are solar wind data from IMP-8 for 30 June 1980. The observed solar wind velocity, on this day was $\tilde{}$ 300 kms^{-1}.[6] This corresponds to an earth-sun flux tube connection at ~W77° while the GRLF occurred at W38°, a difference of 40° in connection longitude.

4. Interplanetary Fluxes and Energy Spectra

An analysis of the GRE γ-ray data from the 3 GRLF indicates that protons were accelerated up to at least 10-20 MeV[4]. While it is not possible here to make a detailed analyses of the flux, energy spectra and anisotropy time histories of the 7 June and 21 June particle events in order to estimate the injected particle population at the sun, we will present particle fluxes and spectral indices γ at the time of maximum particle intensities. This information is given in Table 2. The values here are derived from 3 hour average counting rates. The γ's are calculated from a least squares fit to the equation $J = AE^{-\gamma}$ where E = Energy/nucleon, and J is the differtial intensity. For the 1 July 1980 GRLF only upper limits of the particle flux can be given.

Table 2. Peak Particle Flux and Spectra Indices

Flare Date	Protons $(cm^2\ sec\ str\ MeV)^{-1}$		Electrons $(cm^2\ sec\ str)^{-1}$			Proton γ	Electron γ
	5-10 MeV	10-20 MeV	115-300 keV	300-440 KeV	0.44-1.3 MeV		
7 June	1.5×10^{-1}	6.8×10^{-2}	4.5×10^{3}	3.1×10^{2}	3.7×10^{1}	2.1	3.5
21 June	3.1×10^{-2}	1.8×10^{-2}	6.7×10^{2}	1.5×10^{2}	2.2×10^{1}	1.8	2.5
1 July	$<1.6\times10^{-2}$	$<1.2\times10^{-2}$	<2.5	$<7.6\times10^{0}$	$<1.9\times10^{0}$	-	-

5. Elemental and Isotopic Composition

Because of the low Z > 1 ion flux in both 7 June and 21 June 1980 GRLF associated particle event we are able to determine composition ratios at equal energy per nucleon E, in only one ULEWAT energy range. The relative composition ratios are presented in Table 3.

Table 3. Abundances for γ-ray Line Flares

Flare	Γ(C/O)	Γ(Fe/O)	Γ(^{3}He/^{4}He)
7 June 1980	0.50±0.08[6]	0.027±0.027[6]	<10^{-2}[7]
21 June 1980	0.79±0.32[6]	<0.07[6]	<10^{-1}[7]
August 1972 (1)(2)(3)	0.47±0.04	0.07±0.03[5]	10^{-3}
^{3}He rich[4]	0.23	1.3	>2×10^{-2}
"Normal"[4]	0.54	0.15	<10^{-3}
Photosphere[4]	0.6	0.05	<10^{-4}
Corona[4]	1.0	0.093	<10^{-3}

(1) Date from Pioneer 10 at 2.2 AU for 3-15 August.
(2) Date for 7.5-46.5 MeV/nuc.
(3) Date from Webber et al.[7]
(4) From Gloeckler[8] for 1-20 MeV/nuc.
(5) For Z ≥ 16 ions
(6) For 1-1.8 MeV/nuc.
(7) For 0.7-0.9 MeV/nuc.

For the 7 June event the data are summed from 7 June 1200 to 8 June 2359. For the 21 June period the data are accumulated for only the first event in Figure 1 from 21 June 0000 UT to 22 June 1200 UT. For comparison we have also presented composition ratios from the August 1972 GRLFs, for ^{3}He rich flares, normal composition flares, the photosphere, and the corona.

6. Discussion and Conclusions

We conclude from results presented in Table 3 that neither the 7 June 1980, 21 June 1980 nor the August 1972 GRLF are classifiable as ^{3}He rich or as Fe rich. This is consistent with the plasma instability preheating model of the ^{3}He and Fe rich events discussed by Fisk[9]. We also note that the GRLFs in Table 3 compared to normal composition flares are depleted in Fe relative to O by a factor of 2-3.

Although the intensity of γ-ray line emission at 2.2 MeV from the 1980 GRLFs is the same order of magnitude as that from the August 1972 GRLF, the peak ~10 MeV proton intensities in the two sets of flares differ by many orders of magnitude. Furthermore we have observed several non GRLF associated particle events with ULEWAT in which the peak proton intensity exceeds that of the GRLF associated events by 2 orders of magnitude. If the proton flux difference between events is not due to propagation effects it could indicate that there is little if any relationship between the ion population that give rise to the γ-ray line emission and the ions population that is injected into interplanetary space.

Acknowledgements

This work at the University of Maryland was supported by NASA contract NAS5-20062. This work at the Max-Planck-Institut was supported by the Bundesministerium fur Forschung und Technologie, FRG, contract RV 14-B8/74 and 0101 017-ZA/WF/WRK 175/4. M.E. Pesses has benefitted from several conversations with J.M. Ryan and D.J. Forrest.

References

1. Chupp, E.L. et al. Nature, 241, 5388, 1973.
2. Ramaty, R. et al. Space Sci. Rev., 18, 341, 1975.
3. Hovestadt, D. et al., IEEE Trans. Geos. Elec., GE-16, 166, 1978.
4. Ryan, J.M., Forrest, D.J. and Chupp, E.L., Priv. comm., March 1981.
5. Rust, D., Private Communication, January 1981.
6. Sol. Geophys. Data, 436, 40, 1981.
7. Webber, W.R. et al., Ap.J., 199, 482, 1975.
8. Gloeckler, G., Particle Acceleration Mechanisms in Astrophysics, 58, 1979.
9. Fisk, L.A., Ap.J., 224, 1048, 1978.

TIME AND ENERGY DEPENDENCE OF HEAVY ION ABUNDANCES IN SOLAR FLARE ENERGETIC PARTICLE EVENTS

G.M. Mason[1], H. Weiss[1], G. Gloeckler[1], and D. Hovestadt[2]

[1]Department of Physics and Astronomy, University of Maryland
College Park, MD 20742 USA

[2]Max-Planck-Institut für Physik und Astrophysik
8046 Garching b. München, W. Germany

ABSTRACT

We present examples of the time and energy dependence of the abundances and spectra of the major heavy ions He, C, O and Fe during solar flare events, taken from a survey using the UMD/MPI ULET telescope on IMP-8 during 1973-1977. In some cases, we find time variations in the O/He, O/C and Fe/O ratios which appear to be inconsistent with models based solely on rigidity dependent propagation in the interplanetary medium.

1. Introduction

In recent years, the availability of relatively low threshold (~1-few MeV/nuc) heavy-ion detectors have made possible the first exploratory investigations of heavy-ion abundance variations during individual solar flare events (Armstrong et al. 1976; O'Gallagher et al. 1976; Scholer et al. 1978; vonRosenvinge and Reames 1979). A common, although not universal feature identified in these early studies has been a decrease in the Fe/O ratio (taken at the same kinetic energy/nucleon) following the flare onset, which can be modeled in terms of rigidity dependent propagation in the interplanetary medium when taking account of the partially stripped Fe vs. the (nearly) fully stripped O. However, other abundance variation features have been identified in isolated flare events which do not appear to be as readily understandable, e.g., O/He variations (vonRosenvinge and Reames 1979; Weiss and Mason 1980), and spatial variations (Armstrong et al. 1976).

To form an overview of these abundance variations, we have carried out a survey of 13 major solar particle events during the recent solar minimum (1973-77) using the ULET telescope on IMP-8 (described by Klecker et al. 1977). Several of the flare periods such as July 3-10, 1974, Nov. 6-10, 1974, and Sept. 10-18, 1977, exhibited complex variations of the monitored abundance ratios whose interpretation is not obvious, and which might be caused by some combination of source characteristics along with propagation and shock event effects in the interplanetary medium. The most commonly (though not always) observed trend in the periods is a tendency for ratios of (heavier ion/lighter ion) to decrease as time passes; the rate and magnitude of this decrease depends on the ratio examined. Below we give examples of two relatively simple events which show this behavior. Even in these cases, though, the details of the abundance variations are difficult to understand by considering only the differing rigidities of the particles.

2. Observations for the 20-23 September 1974 Flare

The 20-23 Sept. 1974 particle event was apparently associated with a 1B flare in McMath region 13225 (N08W63) at 2253 on Sept. 19. The upper

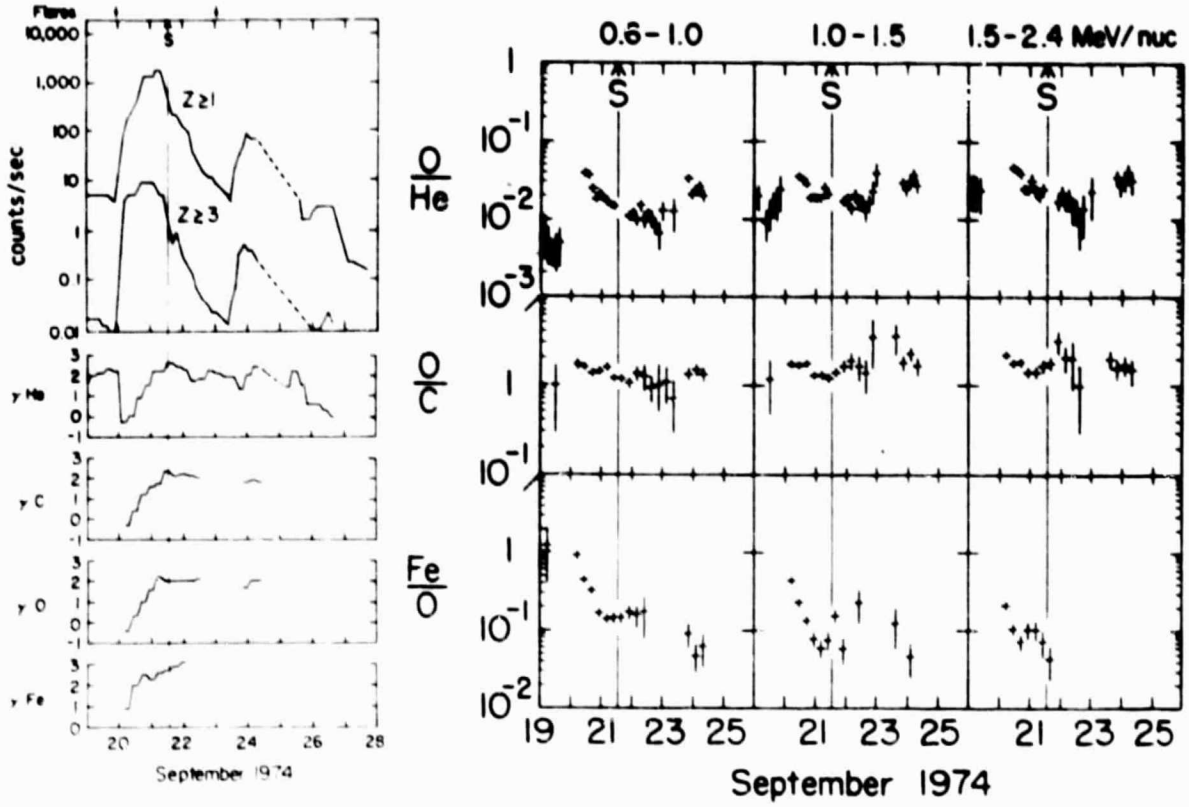

Fig. 1. Count rates, spectral indices and abundance ratios during 19-28 September 1974

left panel of Fig. 1 shows ULET 3-hour average count rates for $Z \geq 1$ and $Z \geq 3$ ions of $\gtrsim$0.5 MeV/nucleon for this event as well as a smaller one starting 23 Sept. (not discussed here). A shock wave, marked S in the fig., passed IMP-8 at 1244 on Sept. 21 (M. Pesses, private communication). The lower left panels of the figure show 3-hr. average spectral indices γ for the monitored fluxes over the range of 0.6-2.5 MeV/nuc, assuming power laws in kinetic energy/nucleon: $dJ/dE = (\text{const})E^{-\gamma}$. The spectral indices show clear velocity dispersion effects, which are not unexpected for a flare of this type, which occurred in the so-called well connected region. Notice however, that major changes in the Fe spectral index γ occur more quickly than for the lighter species, and it is larger at later times than the indices for the lighter species, leading to a decrease in the Fe/O ratio at higher energies which may be easily seen in the plotted abundance ratios. For He, C and O, the changes in γ appear to stop after the shock passage.

The right panels of Fig. 1 show 3-hr. average abundance ratios of (heavier species/lighter species) during this period for each of the 3 energy windows monitored. The figure format for abundance ratios arranges kinetic energy/nuc windows vertically, and ratio types horizontally resulting in 3 repetitions of the time scale. The Fe/O ratio in all energy windows is seen to decrease rapidly (1/e fall-off time $T_0 \sim 12$ hrs) by a factor of $\sim$8 after the flare onset, consistent with rigidity dependent propagation of partially stripped Fe ions as discussed by O'Gallagher et al. (1976) and Scholer et al. (1978) for this event. After this rapid fall off, the time variation becomes less rapid. In the case of the O/C ratio,

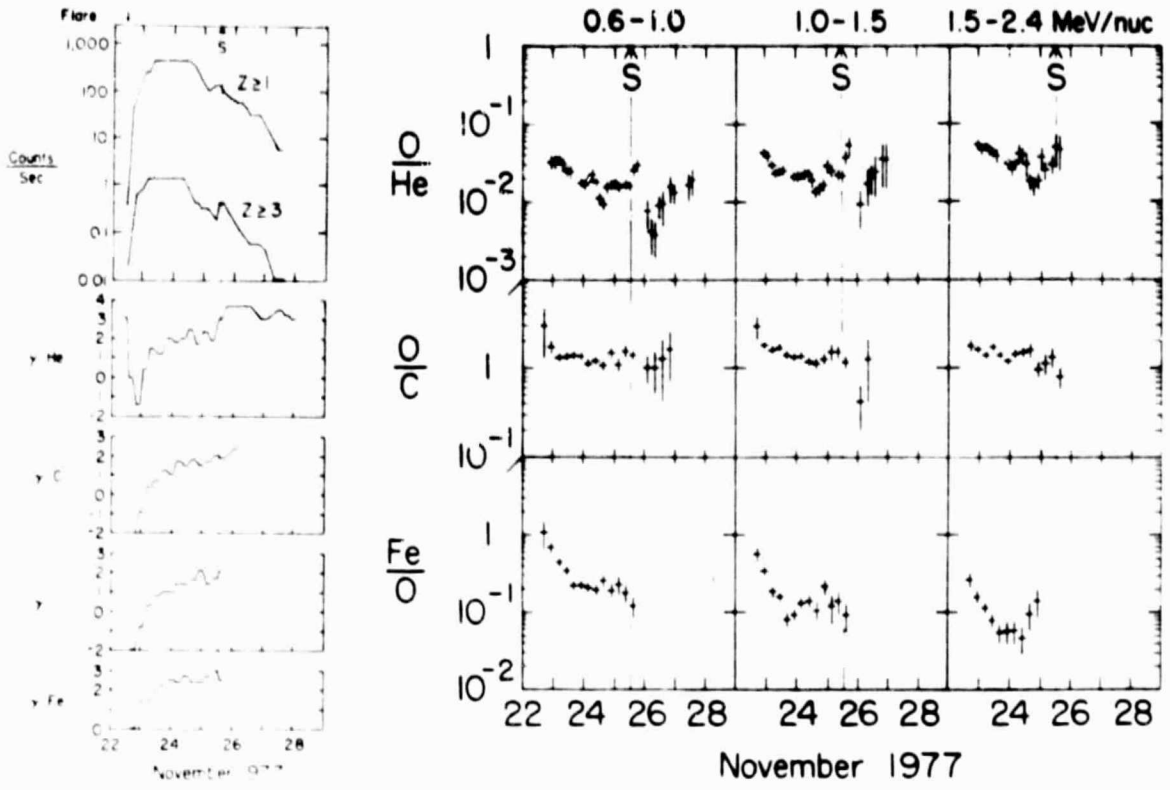

Fig. 2. Observations during 22-29 November 1977

there is also a decrease, at least up to the time of the shock passage, with fall-off time $T_0 \sim 100$ hours. Finally, the O/He ratio is also seen to systematically decrease in time with $T_0 \sim 40$ hrs, and in this case the rate of decrease does not appear to be changed by the shock passage.

3. Observations for 22-26 November 1977

A second example of time dependences of the type discussed above is seen in a November 1977 particle event associated with a 2B flare at 0945 on 22 Nov. in the "well-connected" region at N24W40. A sudden commencement was observed at Earth at 1227 on 25 Nov. Fig. 2 shows the count rates, spectral indices and abundance ratios during this period. Velocity dispersion effects are clearly evident in the spectral index data from the onset time until about 1200 on 23 Nov., after which the spectra continue to steepen, but at a reduced rate. As in the preceding case, the Fe/O ratio quickly drops after the onset ($T_0 \sim 15$ hrs) and then becomes more nearly constant. It is interesting to note in this case that the change in temporal behavior of the Fe/O ratio is not associated with the shock passage, while in the case of the Sept. 1974 event such an association might be inferred. Up to the time of the shock passage, the O/C and O/He ratios decrease in a similar manner to the Sept. 1974 events. There appears to be a definite change in O/C associated with the shock passage.

We emphasize that the time variations in the abundance ratios in this event are not ordered by the individual spectral indices. That is, the time decreases in the ratios do not appear to depend upon the heavier ion

having a steeper (or flatter) spectral slope than the lighter ion, since it can be seen that Fe/O decreases with time with $\gamma_{Fe} > \gamma_O$, while O/He decreases with time with $\gamma_O < \gamma_{He}$.

4. Discussion

The clear velocity dispersion effects seen in these events suggest an interpretation based on propagation effects in the interplanetary medium, where at the same velocity partially stripped Fe has a higher rigidity than nearly stripped O (O'Gallagher et al. 1976; Scholer et al. 1978). In order to examine the new data presented here in this light, we use the most recent observations for solar flare ion charge states for ~1 MeV/nucleon particles, from Hovestadt et al. (1980, 1981) who find mean charge states of He, C, O, and Fe of 1.9,5.8,7.2 and 13.5, respectively. With these charge states, the ratio of particle rigidities at equal velocities are P(O/He)=1.06; P(O/C)=1.07; P(Fe/O)=1.87. Thus, the significantly higher rigidity of Fe vs. O might well lead to more rapid propagation for Fe in a model where the scattering mean free path increases with rigidity, as described in earlier works. However, the O/He and O/C variations are puzzling considering the small rigidity differences of the species, as is the fact that the O/He variations are more similar to the Fe/O than the O/C variations, while consideration of the rigidity ratios would lead to the opposite expectation. We conclude that rigidity differences alone cannot explain the observations presented here.

We speculate that other factors, such as abundance differences at the flare site on the sun, or features of the acceleration and release mechanisms may play an important role in the variations discussed here, as well as the more complex cases in flares cited in §1. We have also found that in general the individual flare spectra are very often not fitted well by the kinetic energy/nucleon power laws used here: not only are the spectral indices for the species often different from each other -- leading to abundance variations at differing energies -- but also the spectra tend to "roll over" towards lower energies. We intend to examine other spectral forms (e.g. distribution functions in particle energy/charge) in order to search for a simpler representation of the data, and to help separate the numerous different effects operating in these particle events.

5. Acknowledgements

We are grateful to the dedicated personnel at the Max-Planck-Institut and the University of Maryland for their excellent work on the IMP-8 experiment. This work was supported in part by NASA contracts NAS5-11063 and NAS5-25735, and grant NGR-21-002-316, and by the German government. One of us (G.M.) thanks the University of Maryland General Research Board for support for a portion of this work.

References

Armstrong, T.P. et al. 1976, Solar Phys., 49, 395.
Hovestadt D. et al. 1980, Space Res./Adv. in Space Expl. (in press) 23, COSPAR.
Hovestadt, D., et al. 1981, submitted to Ap.J. (Letters).
Klecker, B. et al. 1977, Ap.J., 212, 290.
O'Gallagher, J.J. et al. 1976, Ap.J. (Letters), 209, L97.
Scholer, M. et al. 1978, J. Geophys. Res., 83, 3349.
vonRosenvinge, T.T. and Reames, D.V. 1979, 16 ICRC Kyoto, 5, 68.
Weiss, H. and Mason, G.M. 1980, Bull. A.P.S., 25, 597.

OMIT

MEASUREMENTS OF IONIZATION STATES FOR LOW ENERGY HEAVY IONS IN SOLAR FLARE PARTICLE EVENTS

L.S. Ma Sung[1], G. Gloeckler[1] and D. Hovestadt[2]

1. University of Maryland, College Park, MD 20742 USA
2. Max-Planck-Institut fur Extraterr. Physik, D-8046 Garching FRG

ABSTRACT

We examine the distributions of ionization states for flare associated heavy particles ($Z > 2$) between 76 and 1000 keV/charge. The particle data have been collected by the University of Maryland/Max-Planck-Institut Electrostatic Energy-Charge Analyzer (EECA) Experiment on IMP-8. The EECA sensor measures particles in the same energy/charge interval. By examining the particle energy pulse-height distribution, the ionization states of $Z > 2$ ions can be deduced if the elemental abundances are known. We determine the elemental abundances between 1.0-4.6 MeV/nucleon from particle data collected by the Ultra Low Energy Telescope (ULET) on the same experiment. In this energy range, a power law fit to the particle spectra would give energy dependent abundance ratios. However, if the particle distribution function f is plotted as a function of the quantity η, where $\eta = vR^n$, v and R are the particle speed and rigidity respectively, and n is an adjustable parameter, all elements are found to share the same distribution $f \sim e^{-\eta/\eta_0}$ with a common η_0 and n[1] for a given particle event. In this representation, the abundance ratios become independent of the spectral shape and can therefore be applied to the lower energy range of the EECA data. For the ionization-state distribution, we assume that ions are in charge equilibrium at a given coronal temperature[2]. By comparing our data in several energy-per-charge windows with calculated distributions which are produced by folding the instrumental profiles with an incident particle population of given elemental abundances and a charge-state distribution, we can determine the charge distribution characteristic of the particle event and hence deduce the temperature of the source materials and the possible acceleration process for these ions.

1. Gloeckler, G., Weiss, H., Hovestadt, D., Ipavich, F.M., Klecker, B., Fisk, L.A., Scholer, M., Fan, C.Y. and O'Gallagher, J.J., 1981, 17th International Cosmic Ray Conf. (Paris, France), SH 3.1-7.
2. Jordan, C. 1969, Mon. Not. R. Astr. Soc., 142, 501-521.

SH 3.1-7

OBSERVATIONS OF THE IONIZATION STATES OF ENERGETIC PARTICLES ACCELERATED IN SOLAR FLARES

G. Gloeckler[1], H. Weiss[1], D. Hovestadt[2], F.M. Ipavich[1], B. Klecker[2], L.A. Fisk[3], M. Scholer[2], C.Y. Fan[4], and J.J. O'Gallagher[5]

1. University of Maryland, College Park, MD 20742 USA
2. Max-Planck-Institut fur Extraterr. Physik, D-8046 Garching, FRG
3. University of New Hampshire, Durham, NH 03824 USA
4. University of Arizona, Tucson, AZ 85721 USA
5. University of Chicago, Chicago, IL 60637 USA

ABSTRACT

We report results of a survey of ten solar flare particle events in which we measured the ionization states and spectra of 0.3 to 2.4 MeV/nuc He, C, O and Fe. We find He^+ to be present in all events ($He^+/He^{++} \sim 0.1$ to 0.25), and the mean ionization states of C, O and Fe to be high. The distribution functions of He^+, He^{++} and heavier elements are well represented by simple exponentials of the particle speed times its rigidity to a power n, where n is between 0 and 1, and equal e-folding values. Our results are consistent with a model whereby ions are accelerated in the corona by multi-dimensional shocks out of a population taken from both hot ($T_e \gtrsim 2 \cdot 10^6$ K) and cold ($T_e \lesssim 10^5$ K) coronal regions.

1. Introduction

Knowledge of the ionization states of particles accelerated in solar flares is important not only because it provides information about the characteristics of the regions where acceleration takes place but also because it is essential to know the charge to mass ratio of these particles in order to determine the nature of the acceleration and propagation mechanisms. Earlier measurements of charge states of $\lesssim$1 MeV/charge solar flare accelerated ions (e.g. Gloeckler et al.[1,2], Ma Sung et al.[3]) indicated high ionization states, consistent with a coronal material at a temperature of $1\text{-}2 \cdot 10^6$ K. The recent discovery by Hovestadt et al.[4] of a surprisingly large relative abundance of He^+ at higher energies, on the other hand, requires a much cooler source material.

In this brief report we outline results of a survey of 10 solar flare particle events observed over a one year period starting in Sept. 1978, using the ULEZEQ sensor of the Max-Planck-Institut/University of Maryland experiment on ISEE-3 positioned $\sim$0.01 AU upstream of the earth. We find that energetic He^+ is present in all of the flare events examined, being the third most abundant element after H and He^{++}. The mean charge states of C, O and Fe, on the other hand, are consistently high, the average values over all 10 flares being 5.8, 7.1 and 13.5 respectively.

2. Instrumentation

In the ULEZEQ sensor the chemical elements are first identified using pulse-height analyzed signals from the proportional counter (dE/dx element) and the solid state detector (E element) of the dE/dx vs E telescope placed at the exit of an electrostatic deflection system which disperses ions according to their energy per charge. The charge states of a particular element are then determined from the amount of deflection

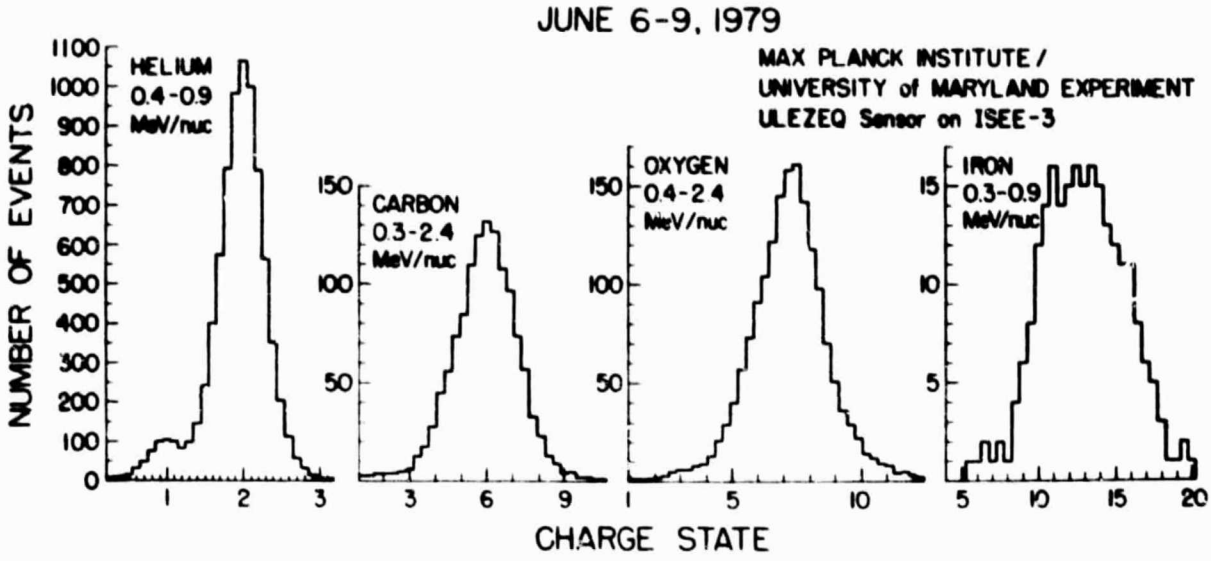

Fig. 1. Ionization state histograms for He, carbon, oxygen and iron for the June 6-9, 1979 solar flare particle event.

measured by a position sensitive detector, and the residual energy E. This analysis is performed for each incoming ion. The instrument and analysis technique are more fully described by Hovestadt et al.[5]

3. Observations

In order to illustrate the results provided by our survey we discuss in some detail particle observations for the June 6-9, 1979 event which are typical of all the flare events examined. Fig. 1 shows the charge state histograms for helium, carbon, oxygen and iron in the indicated energy per nucleon intervals. The resolution of the instrument allows us to separate the individual charge states of He although not of the heavier elements. The He^{+} abundance is about 10% that of He^{++}. The ionization states of the heavier elements are high: the mean charge states of C, O and Fe are 5.7, 7 and 12.5 respectively. Our preliminary analysis does not allow us to estimate the distribution of charge states of each heavy element, although it is evident, especially in the case of iron, that several ionization states are present (e.g. 10 to 15 for Fe). However, we find no evidence in any of the heavy ion charge histograms examined for low ionization states (e.g. O^{+}, Fe^{+3}) above a few percent level. Finally, we point out that our present determination of mean ionization states is subject to systematic errors of $\sim$0.05 of the charge state.

The energy spectra of He^{++}, He^{+}, O, C and Fe are shown for the June 1979 event in Fig. 2(a). In the restricted energy range of 0.3 to 2.4 MeV/nucleon the spectra may be fitted to power-laws, $j = AE^{-\gamma}$. We note, however, that the spectral indices are different (e.g. $\gamma \simeq 1.7$ for He^{++} and 2.2 for Fe) and that the power-law fit is especially poor for He^{++}. In order to find a spectral representation in which the energy dependence of the ratios is removed we show in Fig. 2(b) the dependence of the distribution functions, $f = j/v^2$, on the quantity vR^n where v and R are the speed and rigidity of the ions respectively, and n is a parameter which is adjusted to minimize the energy dependence of the ion abundance ratios. With n = 1/3 for the June event we find excellent fits to all the data, where the distribution function for each species i has the form

$f_i = A_i \exp(-vR^n/E_0)$ with a common $E_0 = 0.26(\text{MeV/nuc})^{2/3}$. In computing the rigidities of O, C and Fe we used mean ionization states derived from the charge histograms of Fig. 1.

A summary of our results for the 10 flare particle events is given in Table 1 which lists the relevant flare characteristics, spectral information, He^+/He^{++} ratios and mean ionization states for C, O and Fe. In the power-law representation of the differential intensities, j, the spectra of He^+ are consistently steeper than those of He^{++} with a flare averaged ratio of the spectral indices $\gamma_{He^+}/\gamma_{He^{++}}$ of 1.17. In a representation where the distribution functions $f \propto \exp(-vR^n/E_0)$, however, one can find values of n for which E_0 is common to He^+ and He^{++}. Typical values for both n and E_0 are $\sim$0.4. Although the He^+/He^{++} ratio is energy dependent when computed at equal energy per nucleon, this ratio is constant in the representation where the species have a common distribution function. Assuming the vR^n dependence of the distribution function is valid over a broader energy range (i.e. $0.1 \lesssim E \lesssim 10$ MeV/nuc) we can derive density ratios for He^+/He^{++} by integrating f over velocity space. These ratios, listed in column 10, are seen to range from $\sim$0.08 to 0.29 with a flare average of 0.15. Finally, the mean ionization states of C, O and Fe, derived from charge histograms such as shown in Fig. 2, are found to be consistently high, in general agreement with previous measurements at lower energies (e.g. Gloeckler et al.[1,2], Ma Sung et al.[3]).

4. Discussion and Conclusion

The fact that energetic He^+ is seen at surprisingly large relative abundances in every solar flare particle event examined indicates its common presence in the source material from which solar particles are accelerated. One plausible explanation of this result and of our finding that

Table 1. Spectral Characteristics and Ionization States of 0.3 to 2.4 MeV/nuc He, C, O and in Solar Flare Particle Events

Flare Characteristics			Spectral Characteristics				Ionization States					
							He^+/He^{++}			Mean Charge States $\langle Q \rangle$[e]		
Date	Importance	Location	$\gamma_{He^{++}}$[b]	$\gamma_{He^+}/\gamma_{He^{++}}$[b]	n	E_0	$r_{E/A}$[b]	r_n[c]	r_ρ[d]	C[f]	O[f]	Fe[g]
1978												
25-27 Sept	3B	W50	1.54	1.05	0.50	0.55	0.06	0.22	0.11	5.7	7.2	13
10-12 Nov	1B[a]	W38	1.82	1.15	0.53	0.33	0.06	0.17	0.08	6.0	7.2	14
1979												
18-22 Feb	1B[a]	W27	2.36	1.06	0.38	0.33	0.06	0.18	0.10	5.7	7.3	15
28-29 Mar	1N[a]	E56	2.25	1.16	0.45	0.37	0.13	0.55	0.29	5.6	6.9	--
3-6 Apr	1B[a]	W14	1.78	1.23	0.47	0.47	0.06	0.17	0.09	5.8	7.2	13
23-25 Apr	?		2.55	1.27	0.71	0.48	0.09	0.50	0.21	6.0	7.2	--
28-30 May	1N[a]	W31	2.42	1.05	-0.05	0.15	0.12	0.09	0.10	5.9	7.2	--
6-9 June	2B	E18	1.66	1.21	0.35	0.42	0.09	0.25	0.14[h]	5.7	7.0	12.5
6-10 July	1N[a]	E52	1.72	1.25	0.42	0.44	0.10	0.33	0.18	5.7	6.9	13
15-26 Sept	3	E107	1.12	1.30	0.60	0.82	0.13	0.50	0.23	5.5	6.7	--
FLARE AVERAGE			1.92	1.17	0.44	0.44	0.09	0.30	0.15	5.8	7.1	13.5

(a) multiple flare injections
(b) energy dependent, averaged over 0.3 to 2.4 MeV/nucleon
(c) ratio at equal $n = vR^n$ (v = velocity, R = rigidity)
(d) density ratio assuming $f = A\exp(-n/E_0)$ holds from $E \gtrsim 0.1$ to $E \gtrsim 10$ MeV/nuc
(e) possibly energy dependent; ratio averaged over 0.4 to 2.4 MeV/nucleon; values subject to systematic error of $0.05\langle Q \rangle$.
(f) one sigma error is $\sim$.15 charge units
(g) one sigma error is $\sim$1.0 charge units
(h) density ratios He^{++}:He^+:O:C:Fe are 55:7:1:0.6:0.16

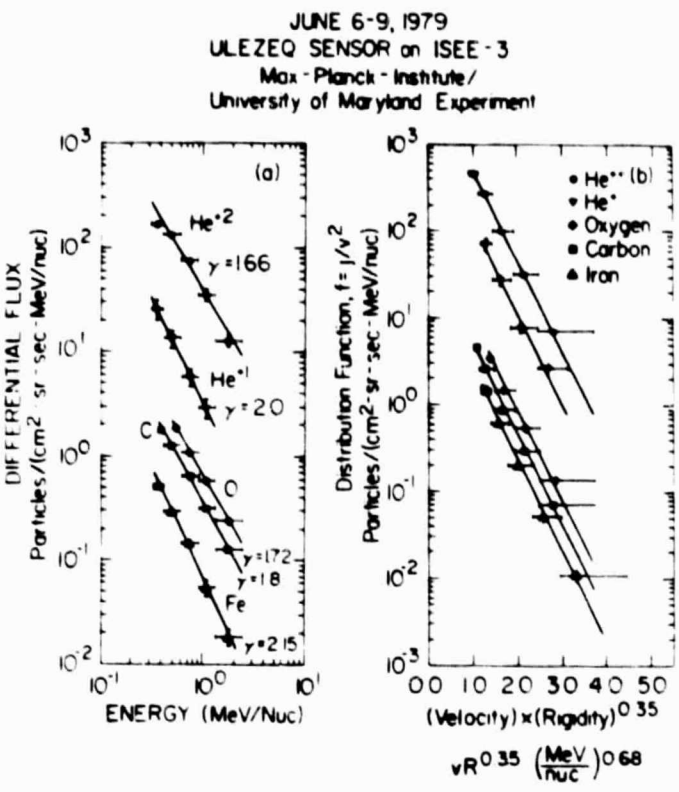

Fig. 2. (a) Energy spectra and (b) distribution functions of He^{++}, He^{+}, O, C and Fe in the June 6-9, 1979 event.

the distribution functions f depend on particle rigidity, is that ions are accelerated by a shock generated as a result of the flare eruption. This shock accelerates material not only from the hot coronal regions (which contain He^{++}, O^{+6-8}, Fe^{+10-15}, etc.) but also from the much colder regions ($T_e \lesssim 10^5$ K) where He^{+}, O^{+} etc. would be present. Cold regions have indeed been observed (Bohlin, private communication), and $f \propto \exp(-vR^n/E_0)$ is consistent with acceleration by multi-dimensional shocks (Lee, private communication). The reason we do not observe low charge states for the heavy elements is that in the limited energy range of our measurements the abundance of singly ionized heavy particles, which have a high rigidity, would be significantly reduced relative to the lower rigidity, highly ionized heavy particles. For example, if we assume for the June 1979 event that f is the same for O^{+} as it is for $O^{+7.4}$, and that the density ratio of "cold" to "hot" material is 0.14 (see column 10 of Table 1), we find that only $\sim$7 O^{+} ions would fall within our energy range. This represents less than 0.5% of the total oxygen population and would be beyond the detection limit of our instrument. This clearly demonstrates the importance of measuring ionization states over a broader energy range with better charge resolution and sensitivity.

5. Acknowledgements

We are grateful to the many individuals in the Space Physics group of the Department of Physics and Astronomy at the University of Maryland, and at the Max-Planck-Institut fur Extraterrestrische Physik who developed the hardware and software of our ISEE experiments. This work is supported in part by NASA under contract NAS5-20062, grants NGR-21-002-224 and NGR-21-002-316, and by the Bundesministerium fur Forschung und Technologie, FRG, contract RV 14B8/74 and 0101 017-ZA/WF/WRK 175/4.

References

1. Gloeckler et al. 1973, 13th ICRC, Denver, 2, 1492.
2. Gloeckler et al. 1976, Ap.J. (Letters), 209, L93.
3. Ma Sung et al. paper SH 3.1-6 this conference.
4. Hovestadt et al. 1981, Ap.J. (Letters)(submitted).
5. Hovestadt et al. 1978, IEEE Trans. of Geosci. Elec. GE-16, 166.

B4

N81-25024

EVOLUTION OF THE ENERGETIC PARTICLE COMPOSITION DURING SOLAR FLARE EVENTS AS OBSERVED BY VOYAGER 1 AND 2

D.C. Hamilton and G. Gloeckler

Department of Physics and Astronomy, University of Maryland
College Park, MD 20742 USA

ABSTRACT

We present measurements of the composition and energy spectra of the energetic ions from two solar flare particle events and discuss their evolution with time during each event. The data are from the Low Energy Particle Telescope (LEPT) on Voyager 2, which can identify the major ion species (Z = 1-26) over an energy range of ~0.5-50 MeV/nucleon.

A prompt particle event resulting from a 2B flare at N23W40 on 22 November 1977 was observed by Voyager 2 at ~1.6 AU from the sun. The event averaged energy spectra (covering 6½ days) of H, He, C, N, O and Fe, for differential flux expressed as a power law in kinetic energy per nucleon, typically have spectral indices in the range 1.5-2.0 from 0.6 to ~2 MeV/nuc and steepen at higher energies. Abundance ratios evaluated at equal energy/nucleon (0.60-0.95 MeV/nuc and 2.1-3.2 MeV/nuc) display the following characteristics: the O/He, O/C, and Fe/O ratios all have maximum values at event onset and decrease fairly smoothly throughout the event, the amount of decrease depending on species and energy. These results are qualitatively similar to those reached from observations at 1 AU in a similar energy range[1]. The behavior of the He/H ratio, however, is more complicated, exhibiting a minimum value (~.014 for 0.60-0.95 MeV/nuc) at onset, increasing to a maximum value (~.067) at time of maximum flux, and then gradually decreasing during the decay phase to a value of ~.029 late in the event.

A large solar particle event was observed by Voyager 2 in September 1979 at ~5.6 AU from the sun. This particle event does not appear to be associated with an optical flare and most likely was produced by a flare on 14 Sept. in McMath region 12698 which was beyond the east limb of the sun at that time (at ~E107°). An X2 x-ray event peaked at 0802 on 14 Sept. and had associated Type II and IV radio bursts. The particle event at 5.6 AU was characterized by hard energy spectra and long duration. Event averaged spectra for H, He, C, N, O, and Fe (covering 17 days) typically have spectral indices in the range 1.3 - 1.7 over an energy range of 0.6 to 20 MeV/nuc, steepening only above ~20 MeV/nuc. In general, the onset portion of the event is complicated, the rise to maximum intensity being dominated by spatial structure rather than IP propagation. Voyager 2 was apparently not well connected to the flare site. The low energy particles (≤a few MeV/nuc) show evidence of enhancement due to passage of at least one IP shock (possibly associated with a CIR) during the event onset. After time of maximum intensity, however, during the relatively smooth decay phase of the event, almost all the abundance ratios of heavier to lighter species (He/H, O/He, O/C, Fe/O) at energies from 0.6 - 1.8 MeV/nuc decrease slowly from their values at maximum intensity to values up to a factor of 2 smaller late in the event.

1. Mason et al., 1981, 17 ICRC Paris, paper 3.1-1.

D5

N81-25025

ON THE ANTICORRELATION BETWEEN THE $^3He/^4He$ RATIO AND PROTON INTENSITY IN ^3He RICH FLARES

M.E. Pesses
Department of Physics and Astronomy, University of Maryland
College Park, Maryland 20742 USA

ABSTRACT

A model is presented which can explain the observed anticorrelation between the size of the $^3He/^4He$ abundance ratio at $\gtrsim$10 MeV/nuc and the peak intensity of $\sim$10 MeV protons in ^3He rich events. If ^3He is preaccelerated with respect to ^4He prior to the main ion acceleration phase, and if the main ion acceleration phase has ar effective injection cutoff which varies from flare to flare, the observed anticorrelation follows naturally.

1. Introduction

Solar flare energetic particle events in which the abundance of ^3He relative to ^4He is enhanced by several orders of magnitude over coronal and photospheric abundances have been the subject of much discussion.[1,2] A particularly interesting feature of the ^3He rich solar flares is the observed occurrence of the largest relative enhancements of ^3He to ^4He in the events in which the peak proton intensity at $\sim$10 MeV is the lowest $\sim 10^{-3}$-10^{-4} protons $(cm^2\ sec\ sr\ MeV)^{-1}$. On the other hand, no ^3He rich flares have been observed in events in which the peak proton intensity is large $\sim 10^{3-4}$ protons $(cm^2\ sec\ sr\ MeV)^{-1}$.

The relationship between the intensity ratio of ^3He to ^4He at equal energy per nucleon $r(^3He/^4He)$, and the peak event intensity of $\sim$10 MeV protons Ip, has been studied by Hempe et al.,[3] and Ramaty et al.[2] The find that over the range of $2\times10^{-2} \lesssim r(^3He/^4He) \lesssim 10^1$ and, $10^{-4} \lesssim Ip \lesssim 10^2$ protons $(cm^2\ sec\ sr\ MeV)^{-1}$ the observations can be fit by a power law, $r(^3He/^4He) = \text{constant} \times Ip^{-\gamma}$ where $\gamma \sim \frac{1}{2}$.

The purpose of this paper is to show that this anticorrelation is a natural consequence of producing abundance enhancement by a two step acceleration process.

2. The Model

The ^3He rich events have been interpreted as being due to the nuclear spallation of $\gtrsim$10 MeV/nuc ^4He into ^3He+n[4,5] and due to the selective heating of ^3He by plasma waves prior to the main acceleration phase[6,7]. The nuclear reaction model is apparently unable to explain either the observed nonenhancement ^2H and ^3H or the observed enhancement of Fe and other heavy ions relative to O in ^3He rich flares.

For this reason I am assuming in this paper that the ^3He enhancements are due to a selective preacceleration of ^3He prior to the main ion acceleration phase. The main ion acceleration phase accelerates ions to the energies at which they are observed in interplanetary space.

A schematic representation of the relative number density of ^1H, ^4He and ^3He prior to the main ion acceleration phase is shown in Figure 1.

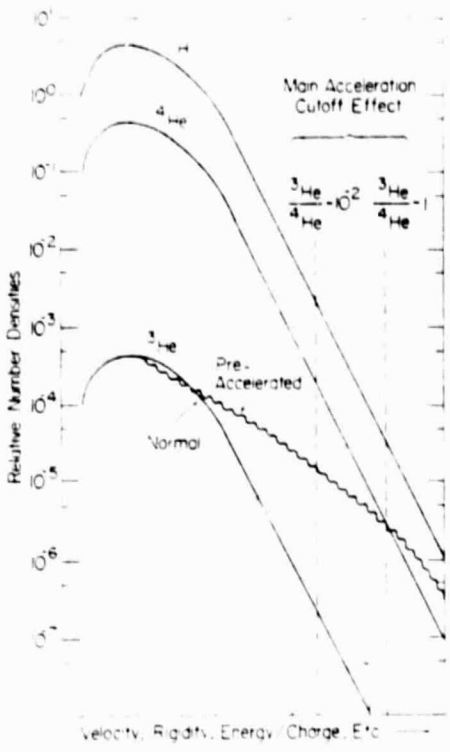

Figure 1

The solid lines are the number densities of ^1H, ^3He and ^4He as a function of some particle variable, like velocity, or rigidity or energy/charge, before pre-acceleration occurs. The wavy line is the number density of ^3He after the pre-acceleration occurs.

The relationship between the number density at the main acceleration site prior to the main acceleration phase n_j and the observed number density of particles at 1 AU n_o can be expressed by using the acceleration-transport particle propagator P, which gives the probability of a particle with some initial value of a variable x between x_j and x_j+dx_j being observed at a value of the variable between x_o and x_o+dx_o. The relationship is given in equation (1) for the case where x = energy/nuc = T.

$$n_o(T_o)dT_o = \int_{T_1}^{T_2} dn_j(T_j)/dT_j P(T_o,T_j)dT_j dT_o \qquad (1)$$

where $n_o(T_o)dT_o$ [$n_j(T_j)dT_j$] is the observed [initial] number density of particles with observed [initial] energy/nuc between T_o and T_o+dT_o [T_j and T_j+dT_j]. The relationship between the observed integral intensity from $T_o = T_1$ to $T_o = T_2$, I_{12} and $n_o(T_o)dT_o$ is given by Equation (2),

$$I_{12} = (4\pi)^{-1}(T_2-T_1)^{-1}\int_{T_1}^{T_2}(2T_o/m_p)^{1/2}n_o(T_o)dT_o \qquad (2)$$

where m_p is the proton mass and the particle observed velocity $\sqrt{2T_o/m_p}$ is << than the speed of light.

As pointed out by Fisk[6], orders of magnitude enhancements in ^3He relative to ^4He can only be produced if there is some cutoff on particle injection into the main ion acceleration phase. If particles of all initial velocity, rigidity, energy per charge etc., have an equal probability of being accelerated to T_o there will be no large ^3He enhancements as the initial and final values of $r(^3He/^4He)$ will be basically the same. There should be some differences in the abundance ratio as most acceleration processes are, in theory, dependent in some fashion on particle mass to charge ratio, which is 3/2 for $^3He^{++}$ and 2 for $^4He^{++}$.

When the injection cutoff is applied to protons as well as helium the observed anticorrelation between $r(^3He/^4He)$ and Ip can be shown to follow naturally.

Assume for algebraic simplicity that $P(T_o,T_j) = (\alpha+1)T_o^{-1}(T_j/T_o)^{\alpha}$ for $T_j \geq T_o$ and zero for $T_j < T_c$ and $T_j > T_o$, where T_c is the injection cutoff energy/nuc, and α is a constant ≥ 0. Also assume for algebraic simplicity that $dn_j(T_j)/dT_j = K(T_j/T^*)^{-\gamma}$, for $T_j > T_c$, where T^* is a constant, and K and γ do not depend on T_j or T^* but can depend on species. Then Equation (1) becomes

$$n_o(T_o)dT_o = \int_{T_c}^{T_o} K(T_i/T^*)^{-\gamma}(\alpha+1)T_o^{-1}(T_i/T_o)^{\alpha}dT_i dT_o \qquad (3)$$

As $T_o \gtrsim 10$ MeV/nuc, T_o is very likely $>>T_c$, which for $\gamma > 1$ reduces (3) to

$$n_o(T_o)dT_o \simeq K(\alpha+1)(\gamma-1-\alpha)^{-1}(T_c/T^*)^{-\gamma}(T_c/T_o)^{\alpha+1}dT_o \qquad (4)$$

Combining (4) with (2) gives,

$$I_{12} \simeq [2\pi\sqrt{2mp}\ (T_2-T_1)(\alpha-\tfrac{1}{2})(\gamma-1-\alpha)]^{-1}(T_1^{\frac{1}{2}-\alpha}-T_2^{\frac{1}{2}-\alpha})K(\alpha+1)T^{*\gamma}\ T_c^{1+\alpha-\gamma} \qquad (5)$$

then $r(^3He/^4He) = I_{12}(\text{for } ^3He) \div I_{12}(\text{for } ^4He)$ which gives

$$r(^3He/^4He) \sim K_3K_4^{-1}(\gamma_4-1-\alpha)(\gamma_3-1-\alpha)^{-1}(T_c/T^*)^{\gamma_4-\gamma_3} \qquad (6)$$

And also $Ip = I_{12}(\text{for } ^1H)$, which gives

$$Ip \sim [2\pi\sqrt{2m}\ (T_2-T_1)(\alpha-\tfrac{1}{2})(\gamma_1-1-\alpha)]^{-1}(T_1^{\frac{1}{2}-\alpha}-T_2^{\frac{1}{2}-\alpha})K_1(\alpha+1)T^{*\gamma_1}T_c^{1+\alpha-\gamma_1} \qquad (7)$$

In (6) and (7) the subscripts 1, 3, and 4 on K and γ refer to the values of K and γ for ^1H, ^3He and ^4He respectively after preacceleration and prior to the main ion acceleration phase. In Equation (6) $\gamma_4 > \gamma_3$.

3. Results and Discussion

Equations (6) and (7) show that as T_c increases in value $r(^3He/^4He)$ increases in value while Ip decreases in size (if $\gamma_1 > 1 + \alpha$), which is consistent with the observed relationship between $r(^3He/^4He)$ and Ip discussed in Section 1. This result can be visualized from Figure 1. As the acceleration cutoff varies in value the number of ^1H, ^3He and ^4He ions which are injected into the acceleration process also varies. Because ^3He has been preaccelerated relative to ^4He, it has harder spectra. Hence as the cutoff velocity, rigidity, energy/charge etc. increases the number of ^3He relative to ^4He that are injected into the main acceleration process increases, while the number of ^1H injected into the main acceleration phase decreases. Since n_o increases as n_i increases the observed anti-correlation between $r(^3He/^4He)$ and Ip follows naturally provided T_c varies from flare to flare. For example, for one value of T_c in Figure 1 $r(^3He/^4He) \sim 10^{-2}$ and for a larger value of T_c $r(^3He/^4He) \sim 1$, with the size of Ip decreasing as the size of $r(^3He/^4He)$ increases.

Acknowledgements

This work was done under NASA contract NAS5-20062 with the University of Maryland.

References

1. Gloeckler, G., Particle Acceleration Mechanisms in Astrophysics, 43, 1979.

2. Ramaty, et al., Solar Flares, 117, 1980.
3. Hempe, H., Mueller-Mellin, R., Kunow, H., Wibberenz, G., 16th ICRC, 5, 95, 1979.
4. Ramaty, R. and Kozlovsky, B., Ap.J., 193, 729, 1974.
5. Colgate, S.A., Andouze, J., and Fowler, W.A., Ap.J., 213, 849, 1977.
6. Fisk, L.A., Ap.J., 224, 1048, 1978.
7. Ibragimov, J.A., Kocharov, G.E., Kocharov, L.G., Dokl. Akad. Novk. SSSR, Joffe Phys. Tech. Inst. Nr. 588, 1978.

D6

N81-25026

ANALYTICAL DESCRIPTION OF CHARGED PARTICLE TRANSPORT ALONG ARBITRARY GUIDING-FIELD CONFIGURATIONS

J.A. Earl
Department of Physics and Astronomy, University of Maryland
College Park, MD 20742 U.S.A.

ABSTRACT

A new description of focused transport has been developed which is valid for arbitrary spatial dependences of both the scattering mean free path and the focusing length. In particular, it describes the "supercoherent transition" from the coherent modes that occur when focusing is strong compared to scattering to the diffusive mode that occurs when focusing is weak. Because it specifies the pitch angle distribution in terms of relatively simple functions, the new formulation facilitates not only the detailed interpretation of solar particle events, but also the qualitative understanding of focused transport. In the steady state, it predicts that the angular distribution consists of a highly collimated "strahl" which is superimposed on an isotropic "halo". This picture provides new insight into observed configurations of steady-state particle fluxes.

1. Introduction. Although particles are clearly scattered by random interplanetary magnetic fields, the mean free path λ during many solar particle events is comparable not only to the distance to the sun, but also to the focusing length L which describes spatial variations of the guiding field B, and which is defined by

$$(1/L) = -(1/B)(\partial B/\partial z), \qquad (1)$$

where z is distance parallel to B. To obtain a better description of the non-diffusive effects that occur under these circumstances, we have analyzed particle transport under the assumption that both the scattering mean free path λ and the characteristic length L for guiding field variations are constant in space and time. (Earl 1976a, 1976b; Bieber 1977) These assumptions do not accurately reflect conditions in interplanetary space, but they drastically simplify the mathematics of the transport problem. This simplified formulation has explained many features of solar particle events (Ma Sung and Earl 1978, Bieber et al. 1979, 1980), but some discrepancies have appeared in the detailed correspondence between theory and experiment. These discrepancies clearly indicate the need for an improved formulation.

In response to this need, Ng and Wong (1979, 1981) and Gombosi and Owens (1980) calculated solar particle fluxes with L dependent upon z. The method introduced by these workers is a valuable contribution, but its purely numerical form encumbers the physical understanding of its implications. Consequently, this paper attempts to provide the insight inherent in an analytic approach by formulating the problem of focused transport in terms of partial differential equations that apply to

arbitrary spatial variations of λ and L. The present analysis follows lines similar to those already taken by Kunstmann (1979), but it differs from his treatment, because it considers two components instead of one, it examines the coupling between these modes, and it includes the effects of spatial variations of λ and L.

2. The New Transport Equations. Particle transport is described, in terms of the distribution function f, by the Boltzmann equation, which can be written in two alternative forms,

$$\frac{\partial f}{\partial t} + \mu V \frac{\partial f}{\partial z} = \frac{1}{2} e^{G} \frac{\partial}{\partial \mu} e^{-G} \frac{\partial f}{\partial \mu}, \quad \frac{\partial (f/B)}{\partial t} + \mu V \frac{\partial (f/B)}{\partial z} = \frac{1}{2} \frac{\partial}{\partial \mu} \phi e^{G} \frac{\partial}{\partial \mu} e^{-G} (f/B), \quad (2)$$

where the odd function G is given by

$$G\{z,\mu\} = -(V/B)(\partial B/\partial z) \int_0^{\mu} (1-\nu^2)(d\nu/\phi\{\nu\}), \quad (3)$$

and where t is time, V is particle velocity, μ is the pitch angle cosine, and $\phi\{\mu,z\}$ is the Fokker-Planck coefficient of pitch angle scattering.

In the calculation of f, it makes no difference which form of the Boltzmann equation is solved, for they are mathematically equivalent. However, certain integrals over the two forms give completely different results. More specifically, the integral over μ of the second form gives the familiar flux equation, which states that the temporal rate at which the density changes is equal to the negative divergence of the flux. If the first form is multiplied by exp{-G} and integrated, the result expresses a similar but less familiar relationship between a weighted density and a weighted flux. Both of these independent relationships must be satisfied by any valid solution of the Boltzmann equation.

A first-order approximation to the distribution function is:

$$f\{\mu,z,t\} = F_{\eta}\{z,t\} + BH_{\xi}\{z,t\} e^{G}. \quad (4)$$

In the steady state with λ and L constant, which represents the zeroth-order situation, the coefficients F_{η} and H_{ξ} are independent of space, time, and each other. Equation (4) describes a slightly perturbed situation in which both coefficients are weakly dependent upon z and t, and in which λ and L are weakly dependent on z. Under these circumstances, the coefficients F_{η} and H_{ξ} cannot be chosen arbitrarily, for the distribution function f must be consistent with the integrals over the Boltzmann equation that were discussed above. This requirement leads to the relationships,

$$\frac{\partial F_{\eta}}{\partial t} - V_{\#} \frac{\partial F_{\eta}}{\partial z} - \frac{B}{K} \frac{\partial}{\partial z} \frac{D}{B} \frac{\partial B}{\partial z} H_{\xi} + \frac{B}{K} \frac{\partial H_{\xi}}{\partial t} = 0, \quad (5)$$

$$\frac{\partial H_{\xi}}{\partial t} + \frac{1}{K} \frac{\partial}{\partial z} V_{\#} K H_{\xi} + \frac{1}{BK} \frac{\partial F_{\eta}}{\partial t} = 0. \quad (6)$$

These are transport equations, whose solutions give a useful description

of particle transport, and in which D is the coefficient of spatial diffusion. Their parameters are given by

$$K = \tfrac{1}{2}\int_{-1}^{+1} e^G \, d\mu, \text{ and } V_{\#} = (V/2K)\int_{-1}^{+1} \mu e^G \, d\mu. \tag{7}$$

Equations (5) and (6) give the familiar phenomenon of diffusion in the weak focusing limit, $(\lambda/L)<<1$, where $V_{\#}\approx(\lambda V/3L)=(D/L)$, but they give essentially coherent transport when focusing is strong, $(\lambda/L)>1$, and $V_{\#}\approx V$. This evolution in structure unfolds continuously as λ and L vary smoothly with z. This means that solutions of the first order transport equations automatically take into account the changes in the qualitative nature of particle transport that occur in physically realistic models of interplanetary conditions. At the Munich conference, for example, I described these changes in terms of a "supercoherent transition" at which the nearly coherent propagation of flare particles in regions of strong focusing near the sun gives way to ordinary diffusion in the outer solar system (Earl 1976b). The new formulation makes it possible to deal with this transition on a quantitative basis.

4. Steady State Solutions. It is not possible to find analytical solutions of the general time-dependent first-order equations. At this stage, numerical methods are appropriate, but they have not yet been implemented. Instead, a simple, new, and general solution of the steady state problem is described below.

In the steady state, the temporal derivatives in equation (6) vanish, and its solution takes the form,

$$H_s = (\sigma/V_{\#}K), \tag{8}$$

where σ is a constant. With this result, equation (5) takes a form,

$$\frac{\partial F_q}{\partial z} = -\frac{B\sigma}{(V_{\#}K)^2}\frac{\partial}{\partial z}\frac{D}{B}\frac{\partial B}{\partial z}, \tag{9}$$

which can readily be integrated to give expressions for the isotropic component F_q.

The figure shows the results of such a calculation for a monopolar guiding field configuration, $B \propto r^{-2}$, in which λ decreases as $\lambda \propto r^{-2/3}$, and into which particles are steadily injected at $r = 0$. Because the ratio $(\lambda/L) = \rho$ decreases with the coordinate r, which replaces z, this configuration embodies a smooth transition from coherent to diffusive transport. The densities, F_q, BKH_s and F_0, are all plotted as ratios to the density F_D predicted under the same circumstances by the diffusion equation. Here, the total density F_0 is the sum of the isotropic density F_q and BKH_s, which is the density embodied in the anisotropic component. The abscissa is the ratio of r to the radius r_0 at which $(\lambda/L) = 1$.

Far from the origin, where $(\lambda/L)<<1$ and transport is essentially diffusive, BKH_s is small compared to F_q and their sum F_0 is identical to

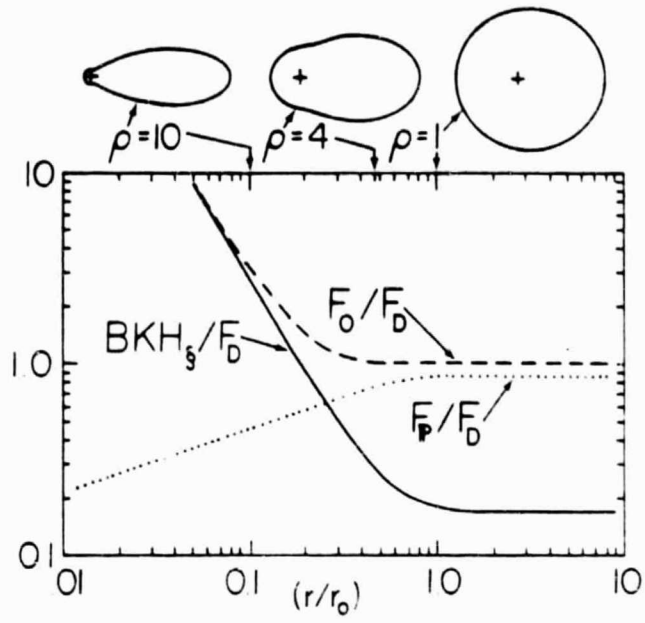

the diffusive result. At the top, a polar plot of the angular distribution $\rho = 1$ exemplifies the relatively weak anisotropies that occur in this region. Near the origin, where $(r/r_0) < 0.1$, transport is nearly coherent, the anisotropic component dominates, and its density is much larger than that predicted by diffusion theory. The strong anisotropies which appear in this region, and which are illustrated by the angular distribution for $\rho = 10$, correspond to a highly collimated beam of particles streaming away from the source.

In the transition region, $0.1 < (r/r_0) < 1$, the density components are comparable, and the angular distributions, as illustrated by the plot for $\rho = 4$, consist of a collimated "strahl" superimposed on an isotropic "halo". These are exactly the features observed aboard HELIOS in the angular distribution of solar wind electrons by Rosenbauer et al. (1977), who interpreted these features in terms of unscattered and backscattered populations of electrons. The present analysis puts this interpretation on a solid analytic foundation, and opens up the possibility of deriving quantitative information from observations of steady-state angular distributions.

Acknowledgements. This research began in Kiel, Germany, where the author was supported by the Alexander von Humboldt Foundation through a senior scientist award and where he benefitted from conversations with G. Wibberenz and J. Kunstmann. In Maryland, its completion was supported by NASA through grant NGR-21-002-066.

References

Bieber, J.W., Ph.D. thesis, University of Maryland (1977).
Bieber, J.W., et al., in Space Research, vol. 19, M.J. Rycroft editor, Pergamon, New York (1979).
Bieber, J.W., et al., J. Geophys. Res. 85, 2313 (1980).
Earl, J.A., Astrophys. J., 205, 900 (1976a).
Earl, J.A., Astrophys. J., 206, 301 (1976b).
Gombosi, T., and A.J. Owens, Astrophys. J., 241, L129, (1980).
Kunstmann, J., Astrophys. J., 229, 812 (1979).
Ma Sung, L.S., and J.A. Earl, Astrophys. J., 222, 1980 (1978).
Ng, C.K., and K.Y. Wong, Proc. 16th Int. Conf. Cosmic Rays, 5, 252 (1979).
Ng, C.K., and K.Y. Wong, Geophys. Res. Letters, 8, 113 (1981).
Rosenbauer, H., et al., J. Geophys., 42, 561 (1977).

D7

A SUPRA-THERMAL ENERGETIC PARTICLE DETECTOR (STEP) FOR COMPOSITION MEASUREMENTS IN THE RANGE ∿20 keV/nucleon to 1 MeV/nucleon

G.M. Mason and G. Gloeckler
Department of Physics and Astronomy, University of Maryland
College Park, Maryland 20742 USA

ABSTRACT

A novel detector system is described, employing a time-of-flight versus residual energy technique which allows measurement of particle composition (H-Fe), energy spectra and anisotropies in an energy range unaccessible with previously flown sensors. Applications of this method to measurements of the solar wind ion composition are also discussed.

1. Introduction

In studies of particle acceleration and transport in astrophysical plasmas, phemonena occurring within our solar system may offer the best hopes of understanding many of the responsible physical mechanisms, since these sources are available for close and detailed observations with numerous information channels. Unlike the cosmic ray accelerators, however, these local sources accelerate particles to modest energies -- usually less than a few MeV/nucleon. Composition measurements of these low energy particles help identify the particle sources; while details of the composition, energy spectra and anisotropies make it possible to distinguish amongst possible models for acceleration and transport. Thus, low energy composition measurements are essential in the study of many particle acceleration sites including, e.g., the solar atmosphere, planetary magnetospheres, interplanetary shock waves, and co-rotating interaction regions.

Previous instruments designed for detailed composition measurements at low energies have employed the dE/dx vs. E technique, wherein the dE/dx detector element was kept as thin as possible in order to achieve a minimum energy threshold. The limits of present technology appear to have been reached with thresholds for, e.g., He of ∿130 keV/nucleon (Krimigis et al. 1977; Hovestadt et al. 1979), and with good resolution of ion species above a few hundred keV/nucleon. In this paper we describe a new technique using measurements of time-of-flight versus energy (Gloeckler 1977; Gloeckler and Hsieh 1979), with which considerably lower energy particles may be studied.

2. Instrumental Technique

Fig. 1 is a cross section of the Supra-Thermal Energetic Particle Detector (STEP), which is one of a pair currently under construction for flight on the Solar Polar Mission. The thin foils and Si detector in the telescope are rectangular (1.5 x 4.0 cm), with the figure showing a cut through the 1.5 cm dimension. The inner foil and solid state detector (SSD) are separated by 10 cm, and define a field-of-view (17° x 44°) with a geometrical factor of 0.4 cm^2-sr.

Ions entering the system pass through the foils and stop in the low-noise SSD. The signal E_{meas} from the SSD is related to the ion energy deposit E by $E_{meas} = \alpha E$, where α is the "defect" in the SSD signal resulting from non-ionizing collisions of the ion with the Si lattice. The

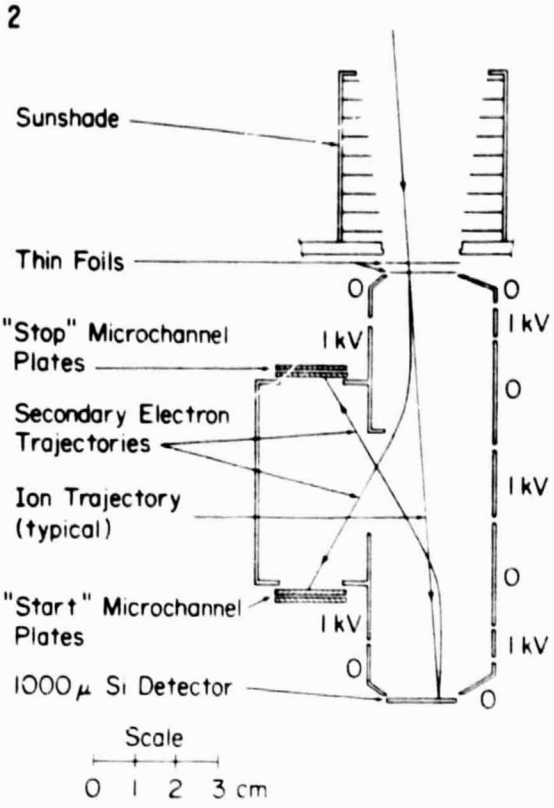

Fig. 1. Simplified cross section view of the STEP telescope

value of α is determined in laboratory calibrations (Ipavich et al. 1978).

In addition to the energy deposit, the ion velocity is measured by making use of secondary electrons which are emitted with a few eV when the ion passes through the surface of the inner foil, and the front of the SSD. The secondary electrons are accelerated to 1 kV, focused, and deflected to hit the surfaces of microchannel plates (MCP) positioned to intercept electrons from the foil ("Start" MCP) or the SSD ("Stop" MCP). The electrostatic acceleration and focusing are done using techniques developed in vacuum-tube technology (e.g. Harman 1953), and avoid the use of accelerating grids. The MCPs produce large, fast signals suitable for determining the ion's time-of-flight, τ, using appropriate fast electronics.

Having measured the particle energy deposit, E_{meas}/α, and time-of-flight (TOF) over a known distance d, the ion mass is obtained from:

$$m = 2(E_{meas}/\alpha)(\tau/d)^2. \qquad (1)$$

The atomic number Z is not determined; however, for all major species over the range H-Fe, a mass measurement is sufficient to identify the ion uniquely. The incident energy of the ion is obtained after taking account of the ion's energy loss in the foils. With this information, plus the known pointing direction of the spacecraft, the composition, energy spectra and anisotropies of the incident ions may be determined.

3. Energy Range and Mass Resolution

The energy range of the STEP telescope for several species is shown in Fig. 2. The lower energy threshold is determined by the SSD discriminator threshold ($\sim$30 keV) and foil thickness. For the STEP telescope, relatively thick foils ($\sim$1500 Å each) are required to limit the sensitivity of the system to solar photons. For applications where sunlight cannot strike the aperture, a very thin foil can be used, yielding considerably lower energy thresholds (see §4). The upper limits of the energy ranges shown in Fig. 2 are set by the threshold value of the time-of-flight electronics ($\sim$3 nsec) for H and He, and by saturation in the SSD amplifiers for heavier species.

It can be seen from equation (1) that the mass resolution of the system is affected by dispersions in E_{meas}, τ and d. For STEP, the major factor below $\sim$1 MeV/nucleon is the dispersion in E_{meas}, resulting from non-ionizing collisions of the ion with the Si lattice. In Univ. of Maryland SSDs similar to those used in STEP, the quantity (FWHM of E_{meas})/E_{meas}

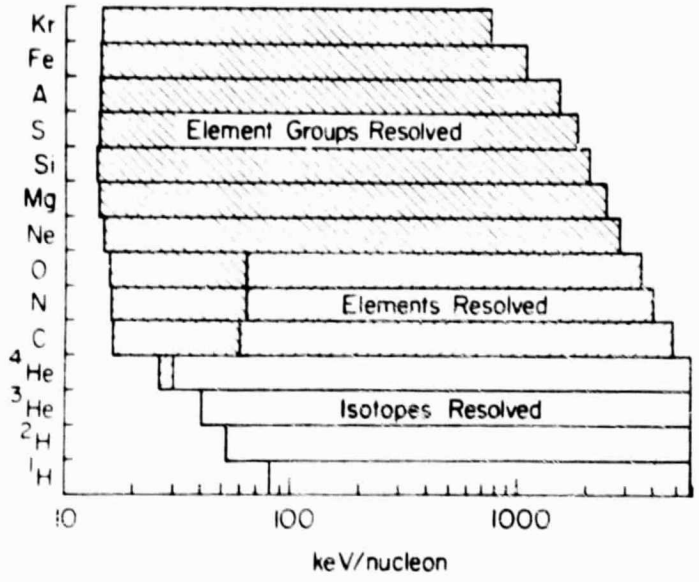

Fig. 2. Energy range of the STEP telescope

increases from a few percent at 100 keV/nucleon to 20-30% near the instrument threshold (Ipavich and Galvin 1980). Taking this effect into account, along with dispersions in τ and d, the instrument is calculated to have regimes of isotope, element and element group resolution as shown in Fig. 2.

Fig. 3 shows the measured mass resolution of the STEP prototype telescope, obtained during its first calibration with heavy ions. For the upper panel, which is typical of energies near threshold, σ_m/m ranges from 0.08 (C) to 0.17 (H). At energies near 200-300 keV/nucleon (lower panel) σ_m/m covers the range from 0.05 (^{3}He) to 0.08 (C). These values were about twice the expected result, due to a crosstalk between the MCPs and the SSD which ~doubled the FWHM of the energy signal in the SSD over the values measured with the same detector when removed from the telescope. It is expected that removal of the crosstalk problem in the flight telescopes will result in the resolution shown in Fig. 2.

The large energy range covered by the STEP sensor, and the mass resolution already achieved in the prototype telescope, show that many hitherto inaccessible regions of the low energy charged particle spectra may be studied for the first time with this instrument.

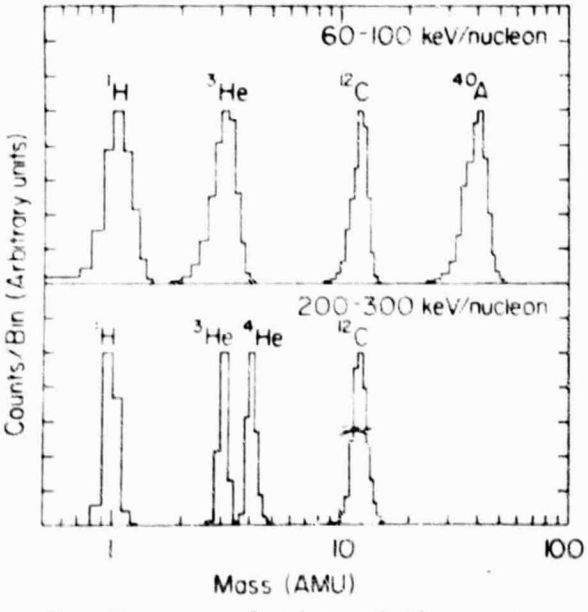

Fig. 3. Mass resolution of the prototype STEP telescope

4. Other Applications

The technique used in STEP may be extended down to solar wind energies, and may include ion charge state determination, by adding features shown in Fig. 4, which is a cross section of the Solar Wind Ion Composition Spectrometer currently under construction for flight on the Solar Polar Mission (Gloeckler et al. 1977). In SWICS, solar wind ions of energy E, mass m, and charge state q enter a collimator and pass through a deflection system whose voltage is stepped through a cycle to select particles of different E/q. The particles are

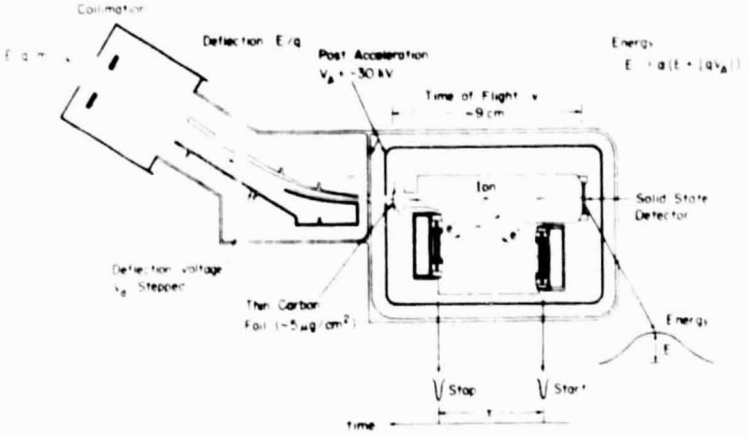

Fig. 4. Cross section of Solar Wind Ion Composition Spectrometer (SWICS).

then accelerated by a voltage V_A(-30 kV) before passing into the TOF system. Sunlight is blocked by the collimator, making it possible to use an extremely thin (~5 μg/cm) mesh-supported carbon foil in the TOF system. After passing through the foil, the particles have an energy $|qV_A| + E'$, where E' is the original energy less the small energy loss of the ion in the foil. As in the case of STEP, the ion's flight time over a distance $\underline{d}$ is measured, as well as the output (E_{meas}) of the SSD. The mass of the ion is then given by equation (1). The ion charge state q is obtained from

$$q = (E_{meas}/\alpha)(|V_A| + E'/q). \qquad (2)$$

The incident energy E is found using the value of q determined in (2), along with the E/q setting of the deflection system. With this information, and the known pointing direction of the spacecraft, the ion's charge state, energy, mass, and arrival direction are determined.

5. Acknowledgements

We are grateful to many individuals in the Space Physics group of the University of Maryland Department of Physics and Astronomy, who are participating in the development of the STEP instrument. One of us (G.M.) wishes to thank the University of Maryland General Research Board for assistance for a portion of this work. This work is supported in part by NASA under grants NGR-21-002-224 and NGR-21-002-316, and NASA/JPL under contracts 955126, 955129, 955460 and 955517. The heavy ion calibration was carried out at the Goddard Space Flight Center van de Graaf.

References

Gloeckler, G. 1977, Univ. of MD. Dept. Physics, Tech. Rept. 77-043.

Gloeckler, G., Geiss, J., Balsiger, H., Fisk, L.A., Gliem, F., Ipavich, F.M., McKenzie, J., Ogilvie, K., Stüdemann, W., and Wilken, B. 1977, "Solar Wind Ion Studies on the Out-of-Ecliptic Mission", proposal to NASA, Aug. 1977.

Gloeckler, G. and Hsieh, K.C. 1979, Nuc. Instr. & Method., 165, 537.

Harman, W.W. 1953, Fund. Electronic Motion, (New York: McGraw Hill).

Hovestadt, D. et al. 1979, IEEE Trans. Geosci. Electr., GE-16, 166.

Ipavich, F.M. et al. 1978, Nuc. Instr. & Method., 154, 291.

Ipavich, F.M. and Galvin, A. 1980 (private communication).

Krimigis, S.M. et al. 1977, Space Sci. Rev., 21, 329.